유체기계연구개발협의회 '97 강연회 및 연구개발 발표회 논문집, pp.13-22
서울대학교 공과대학, 1997. 2. 21.

ON ROTATING CAVITATION

Y.Tsujimoto
Osaka University
Engineering Science
Japan

INTRODUCTION

During the development of the liquid oxygen (LOX) turbopump for the LE-7 main engine of the HII rocket, a supersynchronous shaft vibration caused by rotating cavitation (R.C.) was observed (Kamijo et al.,1993). R.C. is quite different from rotating stall (R.S.): (1) the cavitating region rotates faster than impeller and (2) it occurs near design flow where the head characteristics have negative slope. Although this R.C. was successfully suppressed by a minor modification of the inducer housing, the cause and the fundamental mechanisms of rotating cavitation remained unclear.

It was reported that R.C. was also experienced in the developments of an alternate design of the high pressure oxygen turbopump for the Space Shuttle Main Engine (Ryan et al., 1994) and of the liquid hydrogen turbopump for ARIANE V (Goirand et al.,1992), showing that R.C. is a common problem of modern high-performance turbopumps for rockets.

We herein review studies to date on rotating cavitation to elucidate what research is necessary to obtain a more complete understanding of rotating cavitation.

EXAMPLES OF ROTATING CAVITATION

Although most of the detailed studies are recent, observations of rotating cavitation can perhaps be traced back to a pioneering work of Acosta (1958) on cavitating inducers. He reported that "The alternate blade cavitation appears to propagate from blade to blade in much the same way as propagating stall in cascades" and warned that "In this regime blade forces can be quite high and the various mechanical parts of the pump assembly can be easily excited to resonance." He also reported on various kinds of oscillating cavitation and proposed several methods to suppress them. One of these methods was applied in the HII inducer and found to be effective. Figure 1 is a diagram showing the location of various modes of cavitating flow observed by Acosta (1958).

Rosenmann (1965) reported on rotating radial forces on an inducer and correctly attributed them to rotating cavitation. Figure 2 shows the cavitation performance Ψ_H, the rotational velocity ratio C_s of the force vector which is identical to the propagation velocity ratio $k_R^* = V_p/U_T$, and the normalized radial force C_R. We should note that C_s is slightly lager than 1. He tried to explain rotating cavitation from a standpoint similar to that of conventional rotating stall (Emmons et al., 1955). However, no direct flow observations nor measurements were made.

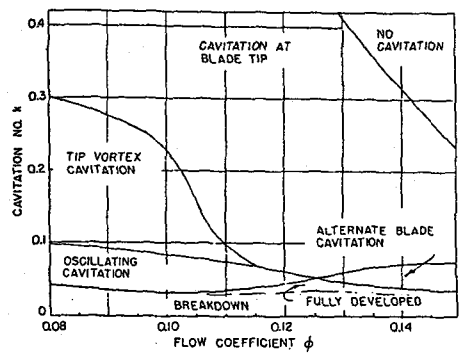

Fig.1 The various modes of cavitating flow in a 12 degs. helical inducer as a function of cavitation number and flow coefficient, from Acosta (1958)

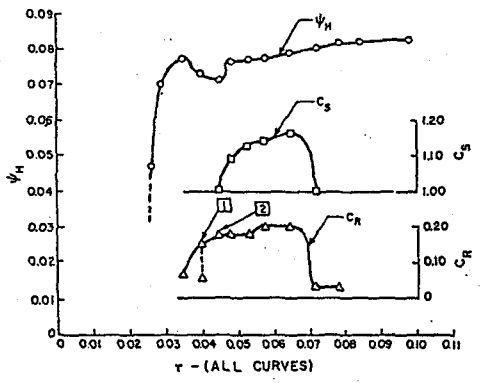

Fig.2 Suction performance ψ_H, rotational velocity ratio C_s of the force vector, normalized radial force C_R plotted against cavitation number τ, from Rosenmann (1965).

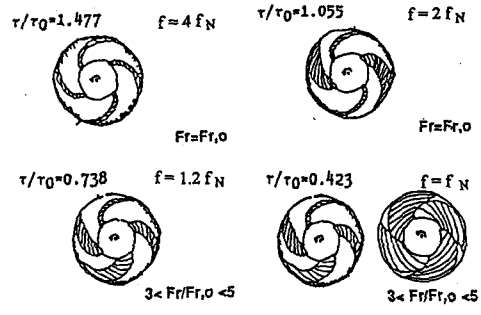

Fig.3 Sketches of cavitated region for various relative cavitation number τ/τ_0, with radial force F_r, non-cavitating radial force F_{r0}, the frequency of pressure oscillation f, and the inducer rotative frequency f_N, from Goirand et al. (1992)

Radial forces on the four-bladed inducer of VULCAIN liquid hydrogen turbopump were reported by Goirand et al.(1992). From flow visualizations, it was shown that stable balanced alternate blade cavitation appears prior to the onset of rotating cavitation as shown in Fig. 3. However, the character of the rotating cavitation was found to be completely the same as that for three-bladed inducers as described in the following section. It was stressed that four-bladed inducers have an advantage as far as the shaft vibrations are concerned, since the alternate blade cavitation does not bring about unbalanced radial forces.

Rotating cavitation occurs not only in inducers but also in industrial centrifugal pumps. Yamamoto(1980) carried out flow measurements and observations in a three-bladed centrifugal pump with a volute suction nozzle. Figure 4 shows the suction performance curve on which the occurrence of flow oscillations is shown. The "heavy oscillation" is caused by cavitation surge and the "weak oscillation" by rotating cavitation, which was identified by visual observation and fluctuating pressure measurements. It was found that the cavitated region rotates slightly faster than the impeller.

It is important to distinguish between rotating cavitation and cavitation in rotating stall. The latter was observed by Murai(1968) on a 18-bladed axial flow pump. Figure 5 shows the head characteristics along with the propagation velocity ratio for three different inlet pressures. We note here that the cavitation in rotating stall occur in the reduced flow range with positive slope of head characteristics and that it rotates with a speed which is 50-60% of the impeller. These characteristics are typical of conventional rotating stall.

CHARACTERISTICS OF ROTATING CAVITATION

Rotating cavitation was first explicitly identified by Kamijo, Shimura, and Watanabe (1977) (see also 1980) and the present section is based on their study. Figure 6 shows the suction performance of the test inducer on which the onset of rotating cavitation is shown. This figure, as well as Figs. 2 and 3,shows that

(1) R.C. is observed in the flow range where the head characteristics have a *negative slope.*

(2) R.C. is observed at the inlet pressure where the cavitation does *not deteriorate the pressure performance* significantly, i.e., above breakdown cavitation number.

Figure 7 shows the sequence of cavity fluctuation on three blades under rotating cavitation. Pictures are shown for every 1/3 turn of the impeller and arranged to shown the size of cavity on each blade at every turn. The blade turns in the sequence of blade 1,2,3 and the time sequence is from left to right. It can be seen that bigger(or smaller) cavities propagate in the direction of blade 3,2,1 and return to the original situation after 4 rotations. This implies *the cavitating region rotates with a speed 1.25 times that of the impeller in the direction of impeller rotation.* This is clearer in Fig 8, in which the lengths of tip and blade surface cavities on each blades, read out from the high speed motion pictures, are plotted against time.

These observations suggest that rotating cavitation is a completely different phenomenon from rotating stall. As

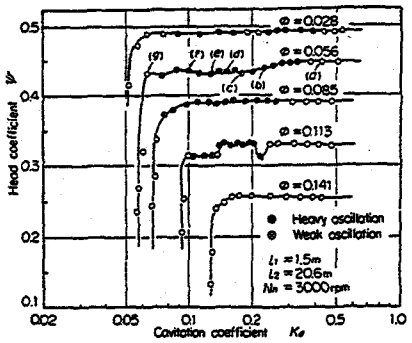

Fig.4 Cavitation characteristics of a centrifugal impeller. Rotating cavitations are shown as "weak oscillation", from Yamamoto (1980)

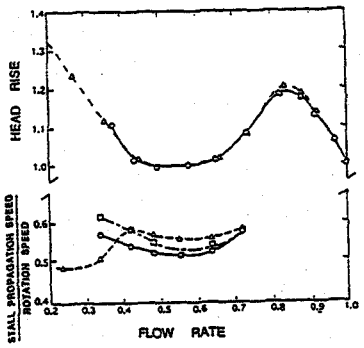

Fig.5 Head characteristics of an axial pump and rotative speed ratio of cavitations in rotating stall, from Murai (1968)

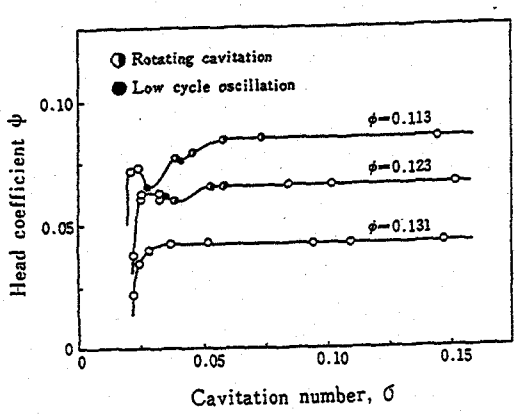

Fig.6 Suction performance of a test inducer

shown in Fig. 5, rotating stalls are *caused by the positive slope* of the performance and the stalled region *rotates slower than the impeller.* On the other hand, it is known that a surge can occur even with negative slope under cavitating conditions. Various terms are used to describe this phenomenon:low cycle oscillations, system oscillations

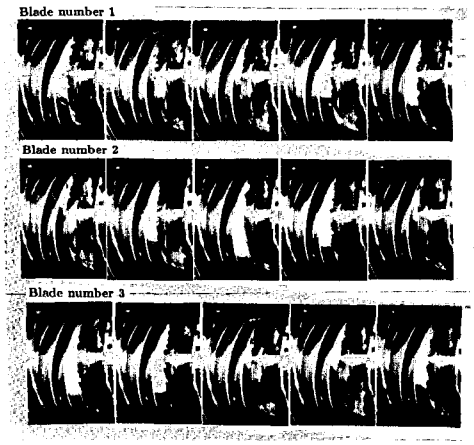

$N = 7,500$rpm, $\sigma = 0.07$, $\phi = 0.118$

Fig.7 Sequence of cavity fluctuations on three blades under rotating cavitation

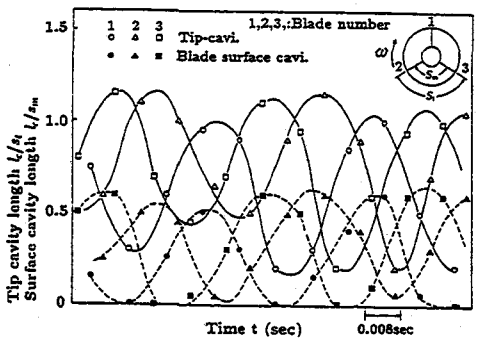

Fig.8 Fluctuations of cavity length due to rotating cavitation

and auto-oscillations with cavitations. The present author believes that it is most appropriate to call them "cavitation surge." It is also known that cavitation surge is caused by a character of cavitation, i.e., a positive mass flow gain factor M, which means that the cavity volume decreases as the flow rate increases. To the author's knowledge, the first systematic explanation of cavitation surge was given by Young(1972), although Sack and Nottage(1965) had succeeded in simulating cavitation surge by a numerical calculation of the system response.

On the other hand, it is also well known (Greitzer,1981) that conventional surge is a one-dimensional, global system instability while rotating stall is a two-dimensional local flow instability, both caused by the positive slope of head characteristics. Now it is quite positive *that rotating cavitation is a local two-dimensional flow instability caused by the positive mass flow gain factor M.* These relationships among flow instabilities in turbomachnery can be summarized as shown in Table 1.

The above discussions can be verified by constructing a flow model which can simulate the above-mentioned characteristics of rotating cavitation.

Table 1 *Relation between flow instabilities in turbomachinery*

Cause and onset flow range	Local instability	System instability
pressure, P — Stall, onset, Design — Flow, Q Positive slope of pressure performance. $\partial P/\partial Q > 0$	Rotating stall	Surge
Cavity volume, V — onset, Design — Flow, Q Positive mass flow gain factor. $M = -\partial V/\partial Q > 0$	Rotating cavitation	Cavitation surge

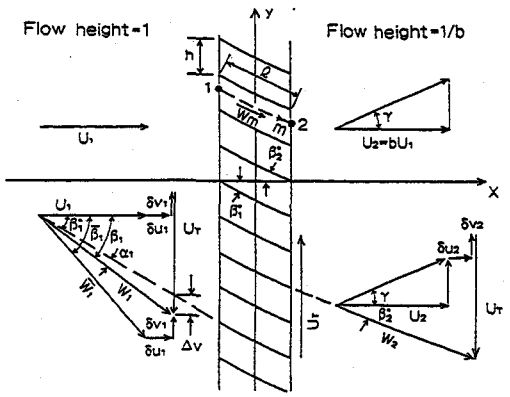

Fig.9 2-D flow model and nomenclature

2-D LINEAR FLOW MODEL

As the simplest possible model of rotating cavitation, a semi-actuator disk model as outlined in Figs. 9 and 10 was constructed (Tsujimoto et al. 1993). The following assumptions have been made.

(a) The flow is inviscid upstream and downstream of the impeller.

(b) Disturbances are much smaller than steady components.

(c) Disturbances change sinusoidally with respect to time t and circumferential coordinate y.

If the flow is assumed to be uniform at upstream infinity, the flow disturbance upstream of the impeller can be expressed by a potential disturbance with an unknown amplitude, A_1. On the other hand, the downstream flow becomes rotational due to the vorticity shed from the impeller. Then the downstream flow field is expressed using two unknown constants, A_2 and C_2, representing the amplitudes of irrotational and rotational disturbances. These three unknown constants are determined from the following three conditions coupling the upstream and downstream flow.

(d) The pressure increase across the impeller. This was estimated by assuming the incidence and through flow losses depending on the incidence at the inlet and the through flow respectively, and also the inertia effects of the fluid in the impeller. No effect of cavitation is assumed for the pressure increase.

(e)The continuity relation across the impeller. We assume that the cavity volume per blade, V_C, is a function of incidence angle α and the local cavitation number $\sigma = (p_1 - p_v)/\rho U_T^2$ and thus $V_C = V_C(\sigma, \alpha_1)$. The continuity relation is obtained by equating the cavity volume change with the axial velocity difference between the inlet and outlet of the impeller, including the cavitation compliance $K = -(\partial V_C/\partial \sigma)/h^2$ and the mass flow gain factor $M = (\partial V_C/\partial \alpha_1)/h^2$ where h is the blade spacing.

(f) Kutta's condition. The relative flow should leave the impeller parallel to the impeller blades.

The conditions (d)-(f) give a set of linear, homogeneous equations with respect to the unknown constants A_1, A_2 and C_2. By equating the determinant of the coefficient matrix with zero, we obtain a third order characteristic equation in terms of a complex propagation velocity ratio $k^* = k_R^* + jk_I^*$, where $k_R^* = V_p/U_T$ is the ratio of propagation velocity V_p to the impeller speed U_T, and k_I^* is the amplifying rate of the disturbance. This is represented by

$$(k^* - k_1^*)(k^* - k_2^*)(k^* - k_3^*) = 0 \qquad (1)$$

Special cases-rotating stall

For the case of $M=K=0$, the characteristic equation (1) can be reduced to a linear equation which yields

$$k^* = \left\{1 - \frac{2\zeta_{ss}\left(1-\tan\beta_1^*/\tan\overline{\beta_1}\right)}{1+b\left(1+\Omega_1'\right)}\right\} + j\left(\frac{b^2/\cos^2\beta_2^* + \mathcal{L}_u}{1+b\left(1+\Omega_1'\right)}\right)\cot\overline{\beta_1} \qquad (2)$$

where,

$$\left.\begin{aligned} \mathcal{L}_u &= 2\zeta_Q + 2\zeta_s\tan\beta_1^*\left(\tan\beta_1^* - \tan\overline{\beta_1}\right) \\ \mathcal{L}_v &= 2\zeta_s\left(\tan\beta_1^* - \tan\overline{\beta_1}\right) \\ \Omega_1 &= 2\pi\left(l^*/s\right)\left(k - \tan\overline{\beta_1}\right) = \Omega_1'\left(k - \tan\overline{\beta_1}\right) \\ l^* &= (1+b)l/\left(2b\cos\overline{\beta}\right),\ \overline{\beta} = \left(\beta_1^* + \beta_2^*\right)/2 \end{aligned}\right\}$$

and ζ_Q and ζ_S are through flow and incidence loss coefficients respectively (see Fig. 9 for nomenclature). It is clearly shown that the propagating velocity ratio k_R^* is smaller than 1. It can also be shown that the onset condition $k_I^* > 0$ can be reduced to the condition where the inlet total to outlet static pressure coefficient has positive slope. Thus, the present model can also simulate rotating stall.

Special cases-rotating cavitation

If we take the limiting cases of $l \to \infty$ or $\beta_2^* \to 90$ degs., the characteristic equation (1) can be reduced to a second order equation. At these limits, axial velocity fluctuation dose not occur at the impeller outlet, due to the infinitely large inertial resistance of the fluid in the impeller or to the negative slope (resistance) of the pressure performance, and hence rotating stall is suppressed. We represent the characteristic equation as

$$(k^* - k_1^{**})(k^* - k_2^{**}) = 0 \qquad (3)$$

It can be shown that the rotating cavitation onset condition for this case is

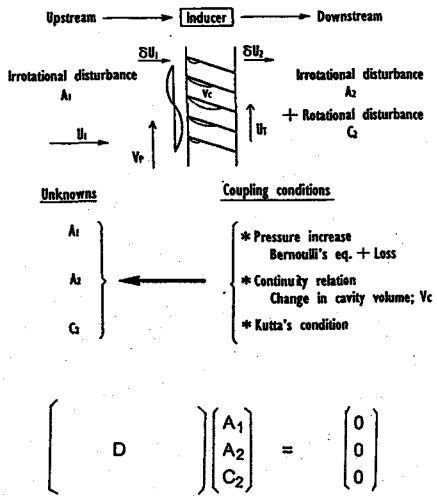

Fig.10 Outline of 2-D linear flow model

Table 2 Results of sample calculations

Values of parameters
β_1^*=77.48°, β_2^*=76.11°
Ω_t' =22.29, Ω_h' =2.09
ζ_Q =1.985, ζ_s =0.612
b =1.24, σ =0.04
ϕ^* =0.794·cot$\overline{\beta}_1$=0.06
K =0.15, M =1.0
k_1^*=(1.277,-0.327)
=(1.239,-0.440)
k_2^*=(-0.526,-2.812)
=(-0.531,-2.815)
k_3^*=(0.957,-0.046)
(0.973,-0.044)

$$M > 2K(1+\alpha)\cot\beta_1 \qquad (4)$$

This clearly shows that rotating cavitation is caused by positive mass flow gain factor M. Furthermore, it can be shown that $k_{R1}'' > 1$ and $k_{R2}'' < 0$, implying that one of the two modes of rotating cavitation rotates faster than impeller and that the other rotates in the opposite direction.

General cases

The results of sample calculations for a typical inducer are shown in Table 2. Solutions of Eq.(1) are shown in the upper lines and those of Eqs.(2) and (3) are shown in the lower lines. It should be noted that:

(a) All of the imaginary parts are negative, showing that both rotating cavitation and rotating stall can occur simultaneously, i.e., they are mutually independent phenomena.

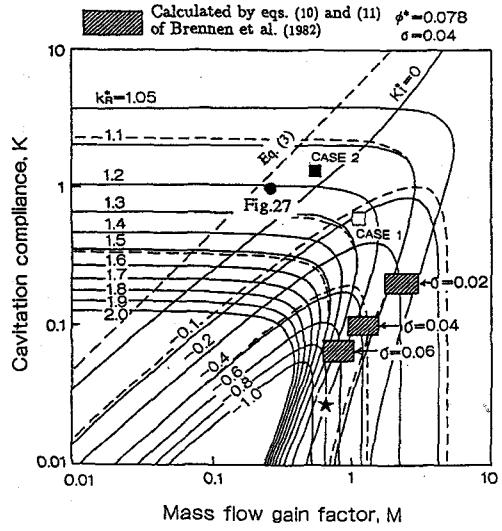

Fig.11 Contour map of k_1*, representing forward rotating cavitation, with real M and K

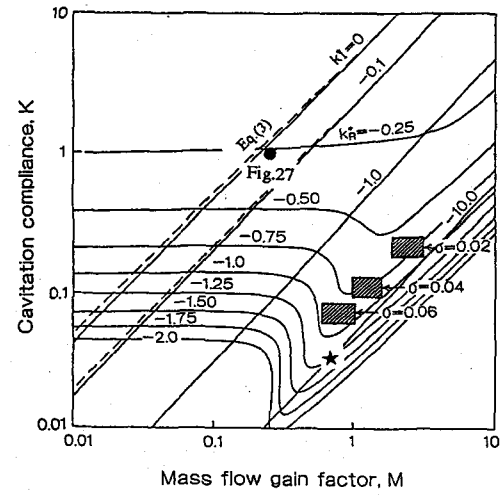

Fig.12 Contour map of k_2*, representing backward rotating cavitation, with real M and K

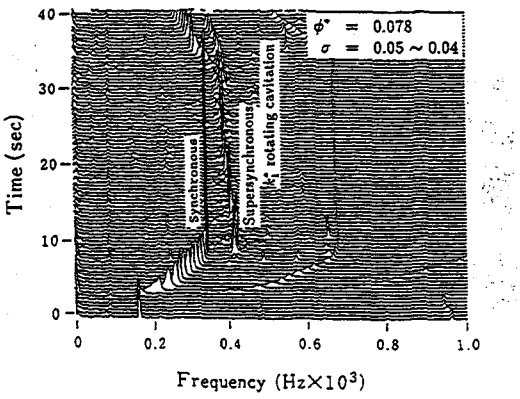

Fig.13 Fourier analysis of LE-7 LOX turbopump shaft vibrations

(b) Three solutions of Eq.(1) have similar values to those of Eqs.(2) and (3). This shows that rotating stall is not significantly affected by cavitation and that the assumptions made for the derivation of Eq.(3) are realistic for typical inducers. The former is verified by the experiments by Murai (1968) as shown in Fig. 5.

In real inducers, however, flow reversal at the inlet tip promotes radial shift of the stream surface at reduced flow rates. As a result, negative slope is obtained throughout the flow range and hence rotating stall seldom occurs.

From the result of further calculations, it was shown that rotating cavitation solutions k_1* and k_2* are mainly dependent on M and K and nearly independent of the flow rate, while the opposite dependence was found for rotating stall solution k_3*.

Figures 11 and 12 show contour maps of k_1* and k_2* in M-K planes for the case of LE-7 LOX turbopump inducer. The solid lines are obtained from Eq.(1), and the broken lines from simplified equation (3). The ranges of M and K estimated from Brennen et al. (1982) are shown in the figures. They are in the amplifying region with negative k_1*, and the propagation velocity ratio k_{R1}* = 1.1-1.2 is in good agreement with the frequency of the shaft vibration data shown in Fig. 13. However, the backward mode corresponding to k_2* is rarely observed in experiments. The example of backward mode is shown in the following section.

Now it is confirmed that *rotating cavitation is a local two-dimensional flow instability caused by the positive mass flow gain factor M* and that the relationships among flow instabilities in turbomachnery can be summarized as shown in Table 1. The mechanisms of the flow instabilities are shown in Fig.14.

By using a similar model, Joussellin and Bernardi (1994) made an attempt to simulate the rotating cavitation in ARIANE V inducer.

BACKWARD ROTATINDG CAVITATION

The experimental observations show that the cavitated region usually propagates in the direction of impeller rotation. The backward mode corresponding to k_2* was recently found at NAL (Hashimoto et al., 1996).

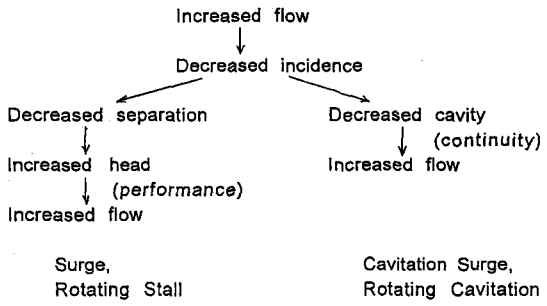

Fig.14 Mechanisms of flow instabilities in turbomachinery.

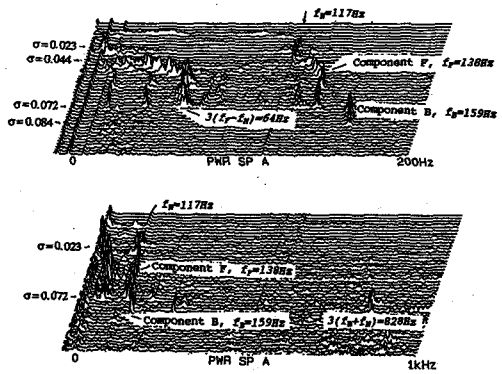

Fig.15 Inlet pressure spectrum of a LE-7 model inducer, with forward and backward rotating cavitation.

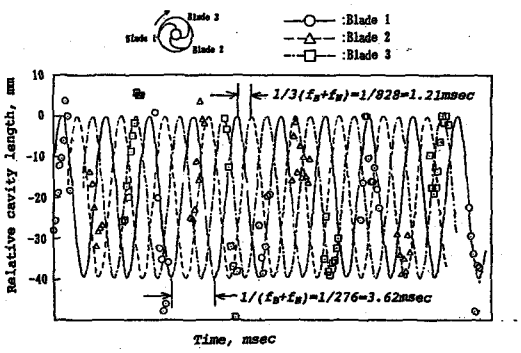

Fig.16 Fluctuation of cavity length due to backward rotating cavitation.

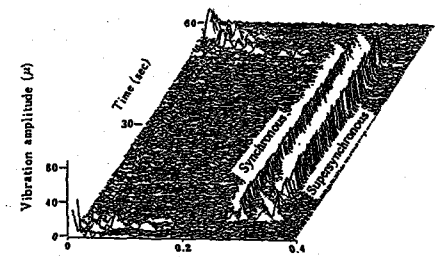

(a) Original inducer housing

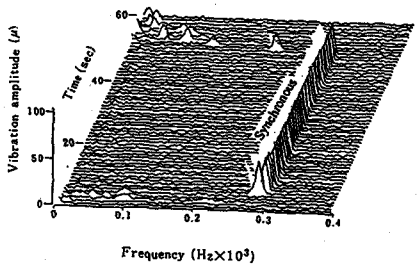

(b) Modified inducer housing

Fig.17 Main pump impeller displacement in LE-7 engine test

Figure 15 shows the spectrum of inlet pressure fluctuation with a LE-7 inducer model at design flow rate. The cavitation number σ is increased from front to back. The shaft rotational frequency is denoted by f_N. We observe two supersynchronous components denoted by F and B. From the phase difference of pressure signals at two different circunferential locations, it was found that the components F and B are caused by forward and backward propagating modes of pressure fluctuation. With the component F (frequency f_F), a component with the frequency $3(f_F-f_N)$ is found. This corresponds to the frequency of the blades to cut the cavitating region which rotates in the same direction as the imeller rotation. Under the occurence of f_B component, a component with $3(f_B+f_N)$, the frequency of the blades to cut the backward rotating cavitation , was found. Thus, the spectrum also shows that the component F is caused by the forward rotating cavitation and the component B by the backward mode. Figure 16 shows the fluctuations of cavity length under the condition with the component B. This also supports the backward propagation. The values of M and K estimated from $k_{1R}^*=f_F/f_N=1.18$ and $k_{2R}^*=f_F/f_N=1.36$ is shown in Figs.11 and 12 by ★ for σ = 0.072. These values are not unreasonable judging from the experimental data by Brennen et al. (1982).

This is the only one example of backward rotating cavitation and we should make further experimental efforts to determine the existence of the backward mode.

SUPPRESSION OF ROTATING CAVITATION

In the development of the LE-7 LOX turbopump, it was possible to suppress rotating cavitation by changing the geometry of the inducer housing (Kamijo et al.,1993), as shown in Fig. 17. The geometry is shown in Fig. 18, and the dimensions are given in Table 3. The CASE 1 is similar to the original housing and the CASE 2 is similar to the modified housing. The values of M and K with these casings were measured by Shimura (1993) and are plotted in Fig. 11. These measurements show that the modification shifts the location of M and K into the attenuating region. However, it is not understood how the geometrical modification changed the value of M and K.

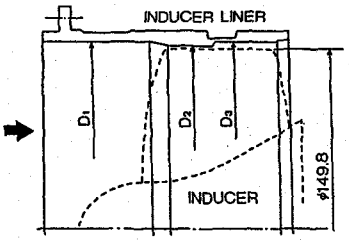

Fig.18 Geometries of inducer housing

Table 3 Dimensions of inducer housing

	Upstream diameter D_1 mm	Front-half diameter D_2 mm	Rear-half diameter D_3 mm
CASE1	150.3	151.0	151.6
CASE2	154.0	151.5	151.5

EXTENSION OF THE ANALYTICAL MODEL

3-D semi-actuator disk model

As shown in Figs. 3 and 7, the flow in the inducer is by no means two-dimensional with large tip cavities. In order to see the effects of the existence of large tip cavities, a 3-D linear flow analysis was made by Watanabe et al. (1995). Their analysis was made for a linear cascade spanning two rigid parallel flat plates simulating hub and casing of an inducer as shown in Fig.19. Here, the flow in the impeller is assumed to be perfectly guided by the vanes and the cavity response is modeled by K and M as in the 2-D flow analysis. The effect of tip cavity is represented by assuming the distribution of K and M as shown in Fig.20. If we represent the flow by using only two radial modes, we obtain a 6th order polynomial characteristic equation. Six roots of this equation correspond to 0th and 1st radial modes of forward and backward rotating cavitation and rotating stall as shown in Table 4.

The contour plots of 0th order rotating cavitation solution are shown in Fig. 21, where $\overline{K}$ and $\overline{M}$ are averaged values of K and M over the span. If we compare the results with those of 2-D flow analysius shown in Figs. 11 and 12, we find that these modes are not largely affected by the uneven distribution of the cavity over the span. This is perhaps the the reason why rotating cavitation with large tip cavities can be simulated by the 2-D model. Similar plot for higher order radial mode show that the 1st order radial modes have larger travelling velocity but the neutral stability curve with $k_1=0$ is nearly the same for all of the modes.

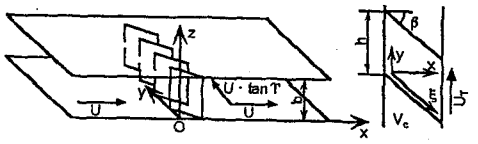

Fig.19 Finite span cascade model.

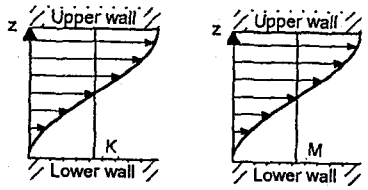

Fig.20 Spanwise distributions of M and K.

Table 4 List of characteristic roots

	Forward R.C.	Backward R.C.	R.S.
0th radial mode	k_{01}*	k_{02}*	k_{03}*
1st radial mode	k_{11}*	k_{12}*	k_{13}*

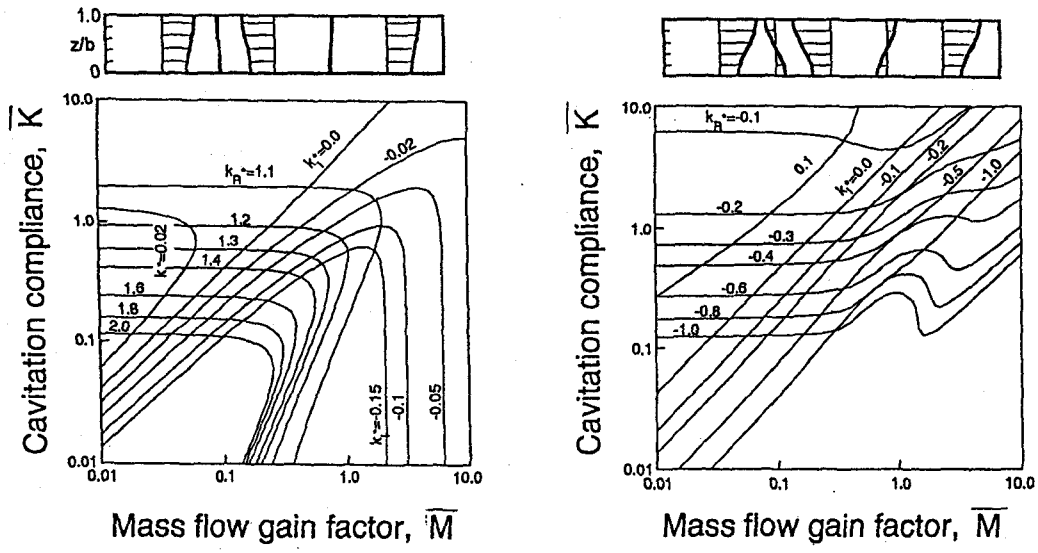

(a) k_{01}*, 0th radial, forward mode

(b) k_{02}*, 0th radial, backward mode

Fig.21 Contour maps of k_1* and k_2*, for a finite span cascade.

2-D finite pitch cascade analysis

So far the cavity is modelled by K and M and no detailed flow around the cavity and the blades is taken into account. This method is useful in elucidating the mechanisms of rotating cavitation but requires to specify the values of M and K.

A detailed flow analysis of cavitating linear cascade as shown in Fig.22 is carried out (Watanabe, 1997). In this analysis the flow is represented by a source distribution q_n on the cavity and vortex distributions γ_{1n}, γ_{2n} and γ_{tn} on the blade and wake surfaces as shown in Fig.23. It is assumed that both steady and unsteady flow disturbances are small. The fluctuation of cavity length is taken into account by specifying the source and vortex distributions using a coordinate stretching with the change of cavity length.

If we apply the pressure boundary condition on the cavity surface and the flow tangency condition on the wetted surface (see Fig.23), we obtain a system of simultaneous integral equations. By discretizing the source and vortex distributions and separating out the unsteady components, the integral equations are converted to homogenious linear equations. The propagating velocity ratio k_R^* and the decay rate k_I^* are determined so that the determinant of the coefficient matrix of the linear equations vanishes.

Figure 24 shows an example of the solutions of k_R^* and k_I^* obtained for a cascade with the solidity C/h=1.88 and the stagger β=79.73 deg, at $\sigma/2\alpha$ =0.25. Five solutions are obtained in the range of k_R^* and k_I^* examined. All modes are amplifying with negative values of k_I^*. The Mode I in the figure corresponds to the forward propagating mode k_{1}^* and Mode II to the backward mode k_2^*. The shape of the cavities for each mode is shown in Fig.25. We find that Mode II and III have higher order fluctuation in the cavity shape.

It was shown that k_R^* and k_I^* are dependent only on the value of $\sigma/2\alpha$, rather than the individual values of σ and α. All modes become destabilizing for smaller values of $\sigma/2\alpha$.

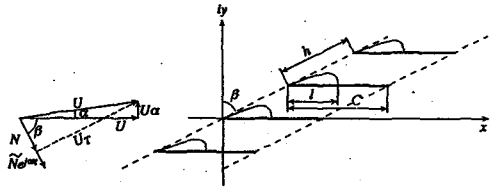

Fig.22 2-D finite pitch cascade model.

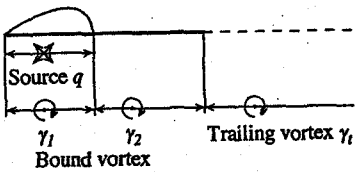

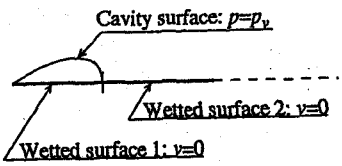

Fig.23 Singularity distributions and boundary conditions.

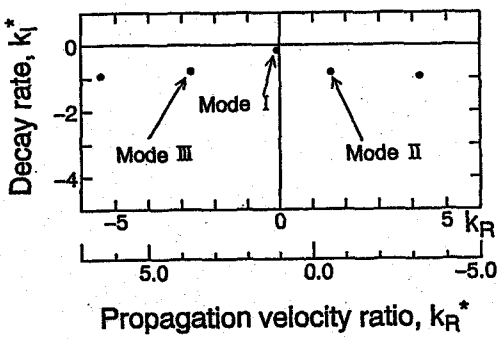

Fig.24 Characteristic solutions for a finite pitch cascade.

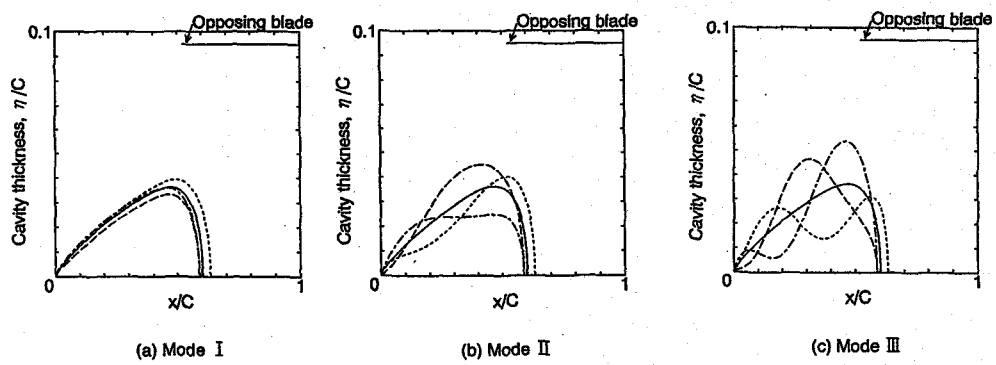

Fig.25 Fluctuation of cavity shape.

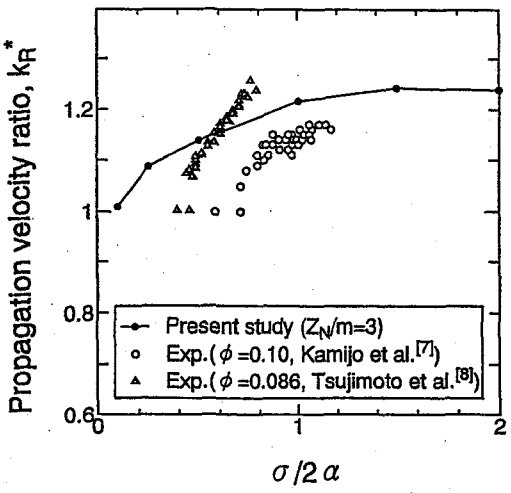

(a) Mode I (forward rotating cavitation)

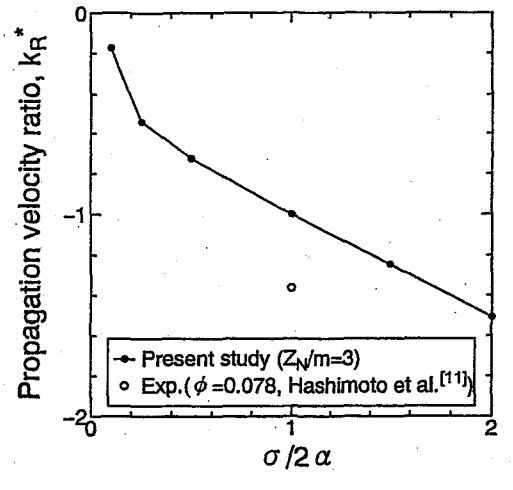

(b) Mode II (backward rotating cavitation)

Fig.26 Propagation velocity ratio k_R^* of a finite pitch cascade.

Figure 26 compares the propagation velocities for the forward mode (Mode I, Fig. 26(a)) and the backward mode (Mode II, Fig. 26(b)). Although the agreement with experiments is only qualitative, the tendency of smaller k_R^* for smaller σ for forward mode is simulated by the model. The largest difference is that the critical value for $\sigma/2\alpha$ is about 1 by experiment while that by the model is about 3.5.

CONCLUSION

It was shown that *rotating cavitation is a two-dimensional flow instability caused by positive mass flow gain factor* M and that the turbomachnery instabilities can be summarized as shown in Table 1. However, many questions remain unanswered and further studies as follows are needed to obtain a more complete understanding of rotating cavitation.

(1) Although the existence of backward propagating rotating cavitation has been experimentally shown, its occurrence is at least far more limited than expected. Further research work is needed to explain the much less possibility of backward propagating mode.

(2) Tip leakage cavitation is predominant in rotating cavitation, as shown in Fig. 6. Studies are needed to determine the dynamic characteristics of this type of cavitation.

(3) Rotating cavitation was suppressed by a minor modification of inducer housing. It was shown that this modification shifted M and K into the attenuating region. Physical explanations should be given for this change of M and K.

(4) The possibilities of higher order modes were predicted in the 3-D flow analysis and the finite pitch cascade analysis. Detailed experimental observations are required to determine the existence of these modes.

The author would like to express his sincere gratitudes to Prof. Kang-Rae Cho of Yensei University for his kind invitation for the presentation of the present paper. The acknowledgements are also to to Prof. K. Kamijyo of Tohoku University who lead the author to the exciting problem of rotating cavitation.

REFERENCES

Acosta, A. J., 1958, "An Experimental Study of Cavitating Inducer," Proceedings of the Second Symposium on Naval Hydrodynamics, ONR/ACR-38, pp.537-557.

Brennen, C. E. and Acosta, A. J. , 1976, "The Dynamic Transfer Function for a Cavitating Inducer," ASME Journal of Fluids Engineering, Vol.98, No. 2, pp.182-191.

Brennen, C. E., Meissner, C., Lo., E. Y. and Hoffman, G. S., 1982, "Scale Effects in the Dynamic Transfer Function For Cavitating Inducers," ASME Journal of Fluids Engineering, Vol. 104, No. 4, pp.428-433.

Emmons, H. W., Pearson, C. E. And Grant, H. P., 1955, "Compressor Surge and Stall Propagation," Trans. ASME, 79, pp.455-469.

Goirand, B., Mertz, A-L., Joussellin, F. and Rebattet, C., 1992, "Experimental Investigations of Radial Loads Induced by Partial Cavitation with a Liquid Hydrogen Inducer," IMechE, C453/056, pp.263-269.

Greitzer, E. M., 1981, "The Stability of Pumping Systems - The 1980 Freeman Scholar Lecture," ASME Journal of Fluids Engineering, Vol. 103, No. 2, pp.193-242.

Hashimoto, H., Yoshida, M., Watanabe, M., Kamijyo, K., and Tsujimoto, Y., 1996, "Experimental Study on Rotating Cavitation of Rocket Propellant Pump Inducers, AIAA 96-2674, to appear in AIAA Journal of Propulsion.

Iacopozzi, M., Lingnaporo, V. and Preval, D., 1993, "POGO Characteristics of ARIANE V Turbopump LOX Pump Inducer," AIAA Paper 93-2124.

Joussellin, F. And Bernardi, J., 1994, "Analitical Modelling of Instabilities in a Cavitating Turbopump Inducer," Proceedings of the Second International Symposium on Cavitation, Tokyo, Japan, pp.89-94.

Kamijo, K., Shimura, T. and Watanabe, M., 1977, 1980, "An Experimental Investigation of Cavitating Inducer Instability," ASME Paper 77-WA/FW-14, and also "A Visual Observation of Cavitating Inducer Instability," NAL TR-598T.

Kamijo, K., Yoshida, M. and Tsujimoto, Y., 1993, "Hydraulic and Mechanical Performance of LE-7 LOX Pump Inducer," AIAA Journal of Propulsion and Power, Vol. 9, No. 6, pp.819-826.

Kim, J. H. and Acosta, A. J., 1975, "Unsteady Flow in Cavitating Turbopumps," ASME Journal of Fluids Engineering, Vol. 17, No. 4, pp.412-418.

Moore, F. K. and Greitzer, E. M., 1986, "A Theory of Post-Stall Transients in Axial Compression Systems, Part I", ASME Journal of Engineering for Gas Turbines and Power, Vol. 108, pp.68-76.

Murai, H. And Takeuchi, H., 1968, "Observations of Cavitation and Flow Patterns in an Axial Flow Pump at Low Flow Rates (in Japanese)," Mem. Inst. High Speed Mech., Tohoku Univ.. 24, No. 246, pp.315-333., also see Brennen, C. E., 1994, Hydrodynamics of Pumps, Concepts ETI and Oxford University Press.

Otsuka, S., Tsujimoto, Y., Kamijo, K. and Furuya, O., 1994, "Frequency Dependence of Mass Flow Gain Factor and Cavitation Compliance of Cavitating Inducers," ASME FED-Vol. 190, pp.119-126.

Rosenman, W., 1965, "Experimental Investigation of Hydrodynamically Induced Shaft Forces with a Three-Bladed Inducer," Proceeding of the Symposium on Cavitation in Fluid Machinery, ASME Winter Annual Meeting, pp.172-195.

Ryan, R. S., Gross, L. A., Mills, D. and Mitchell, P., 1994, "The Space Shuttle Main Engine Liquid Oxygen Pump High-Synchronous Vibration Issue, the Problem, the Resolution Approach, the Solution," AIAA 94-3153.

Sack, L. E. And Nottage, H. B., 1965, "System Oscillations Associated with Cavitating Inducers," ASME J. Basic Eng., Vol. 87, pp.917-924.

Shimura, T., 1993, "The Effects of Geometry in the Dynamic Response of the Cavitating LE-7 LOX Pump," AIAA 93-2126.

Tsujimoto, Y., Kamijo, K., Yoshida, Y., 1993, "A Theoretical Analysis of Rotating Cavitation in Inducers," ASME Journal of Fluids Engineering, Vol. 115, No. 1, pp.135-141.

Tsujimoto, Y., Watanabe, S., Kamijo, K. and Yoshida, Y., 1994,"A Non-linear Calculation of Rotating Cavitation in Inducers," ASME Journal of Fluids Enjineering, 118-2, pp.589-594.

Tsujimoto, Y., Yoshida, Y., Maekawa, Y., Watanabe, S, and Hashimoto, T., 1995, "Observations of Oscillating Cavitations of an Inducer," ASME FED-Vol.226, pp.127-134, to appear in the Journal of Fluids Engineering

Watanabe, S., Yokota, K. And Tsujimoto, Y., 1995, "A Linear Analysis of Rotating Cavitation in a Finite-Span Cascade," Trans. JSME B 61-591,(in Japanese), pp.3900-3907.

Watanabe, S., 1997 "Theoretical Study of Rotating Cavitation" Ph.D thesis, Engineering Science, Osaka University.

Yamamoto, K., 1980, "An Experimental Study on Instability in a Cavitating Centrifugal Pump with a Volute Suction Nozzle," Proceedings IAHR Symposium, Tokyo, pp.303-312.

Young, W. E., et al., 1972, "Study of Cavitating Inducer Instabilities, Final Report", NASA CR-123939.